Published in final edited form as:
J Control Release. 2013 February 28; 166(1): 66–74. doi:10.1016/j.jconrel.2012.12.009.

Synthesis and Evaluation of a Backbone Biodegradable Multiblock HPMA Copolymer Nanocarrier for the Systemic Delivery of Paclitaxel

Rui Zhang[1,a], **Kui Luo**[1,a], **Jiyuan Yang**[1], **Monika Sima**[1], **Yongen Sun**[2], **Margit M. Janát-Amsbury**[2], and **Jindřich Kopeček**[1,3,*]

[1]Department of Pharmaceutics and Pharmaceutical Chemistry/CCCD, Bioengineering, University of Utah, Salt Lake City, Utah, 84112, USA

[2]Department of Obstetrics and Gynecology, Bioengineering, University of Utah, Salt Lake City, Utah, 84112, USA

[3]Department of Bioengineering, University of Utah, Salt Lake City, Utah, 84112, USA

Abstract

The performance and safety of current antineoplastic agents, particularly water-insoluble drugs, are still far from satisfactory. For example, the currently widely used Cremophor EL®-based paclitaxel (PTX) formulation exhibits pharmacokinetic concerns and severe side effects. Thus, the concept of a biodegradable polymeric drug-delivery system, which can significantly improve therapeutic efficacy and reduce side effects is advocated. The present work aims to develop a new-generation of long-circulating, biodegradable carriers for effective delivery of PTX. First, a multiblock backbone biodegradable *N*-(2-hydroxypropyl)methacrylamide(HPMA) copolymer-PTX conjugate (mP-PTX) with molecular weight (Mw) of 335 kDa was synthesized by RAFT (reversible addition-fragmentation chain transfer) copolymerization, followed by chain extension. *In vitro* studies on human ovarian carcinoma A2780 cells were carried out to investigate the cytotoxicity of free PTX, HPMA copolymer-PTX conjugate with Mw of 48 kDa (P-PTX), and mP-PTX. The experiments demonstrated that mP-PTX has a similar cytotoxic effect against A2780 cells as free PTX and P-PTX. To further compare the behavior of this new biodegradable conjugate (mP-PTX) with free PTX and P-PTX *in vivo* evaluation was performed using female nu/nu mice bearing orthotopic A2780 ovarian tumors. Pharmacokinetics study showed that high Mw mP-PTX was cleared more slowly from the blood than commercial PTX formulation and low Mw P-PTX. SPECT/CT imaging and biodistribution studies demonstrated biodegradability as well as elimination of mP-PTX from the body. The tumors in the mP-PTX treated group grew more slowly than those treated with saline, free PTX, and P-PTX (single dose at 20 mg PTX/kg equivalent). Moreover, mice treated with mP-PTX had no obvious ascites and body-weight loss. Histological analysis indicated that mP-PTX had no toxicity in liver and spleen, but induced massive cell death in the tumor. In summary, this biodegradable drug delivery system has a great potential to improve performance and safety of current antineoplastic agents.

*Corresponding author: Jindřich Kopeček, Center for Controlled Chemical Delivery, 20 S 2030 E, BPRB 205B, University of Utah, Salt Lake City, UT 84112-9452, USA. Phone: (801) 581-7211; Fax: (801) 581-7848. jindrich.kopecek@utah.edu (J. Kopeček).
[a]R.Z. and K.L. contributed equally to this work.

Keywords

N-(2-hydroxypropyl)methacrylamide (HPMA); biodegradable multiblock copolymer; paclitaxel; ovarian cancer

1. Introduction

Current regimens of cancer chemotherapy are still far from satisfactory – their efficiency is limited, drug resistance by cancer cells exists, and patients suffer from adverse side effects. It has been realized that the inefficiency, drug resistance, and side effects in current chemotherapy are caused mainly by unsatisfactory formulation, pharmacokinetics, and biodistribution of antineoplastic agents [1]. In general, most drugs are quickly distributed throughout the body after intravenous administration, with no selectivity towards the tumor, which to a great extent confines their efficacy. To increase the exposure time of tumor cells to drugs, current chemotherapy is given intermittently, with periodic injections/infusions. Thus, it is desirable to develop new strategies to radically change performance and safety of current chemotherapy, particularly through the transformation of drug formulations.

Paclitaxel (PTX), one of the most active antineoplastic agents, binds to the subunit of the tubulin heterodimer, resulting in the arrest of the cell division cycle between the prophase and anaphase, and ultimately apoptosis of cancer cells [2]. It has exhibited a significant therapeutic effect against various tumors, including ovarian, breast, non-small cell lung, and head and neck carcinomas [3–7]. However, its low water-solubility (0.25 μg/mL) requires co-injection in a vehicle composed of Cremophor EL® (polyethoxylated castor oil) and ethanol, causing severe hypersensitivity reactions [7–9]. Over the past decade, a number of drug delivery systems have been developed to improve formulation of PTX, such as lipid- or polymer-PTX conjugates [10–17]. Although some polymeric formulations have shown great potential [13, 14, 17], there still is room for improvement. The molecular weight (Mw) of currently used HPMA copolymer-drug conjugates (first generation) is suboptimal - the renal threshold limits the Mw below approximately 50 kDa (the cutoff depends on carrier architecture, molecular weight, hydrophobicity of side chain termini substituents, and conformation [18–21]), which lowers the retention time of the conjugate in the circulation with concomitant decrease in pharmaceutical efficiency. To address this issue, long-circulating polymeric drug carriers with higher Mw have to be developed. Considering that high Mw polymer with a non-degradable backbone will deposit in normal organs and impair biocompatibility, the concept of backbone biodegradable copolymer carriers is advocated [22–28].

In this study, we developed a new-generation of multiblock backbone biodegradable HPMA copolymer-PTX conjugate with relatively high Mw. Both *in vitro* and *in vivo* evaluations were performed to compare the behavior of this new generation conjugate with free PTX and first generation low Mw HPMA copolymer-PTX conjugate, including cytotoxicity, pharmacokinetics, biodistribution, single photon emission tomography/computed tomography (SPECT/CT) imaging, antitumor activity, toxicity, and histological analysis. We found that the new generation conjugate exhibited enhanced therapeutic efficacy and reduced toxicity as compared to the first generation conjugate and free PTX. In addition, *in vivo* biodegradation of multiblock polymer carrier was demonstrated by SPECT/CT imaging and biodistribution study. Thus, the new multiblock HPMA copolymer-based nanocarrier with high Mw is considered a promising drug-delivery candidate to improve performance and safety of PTX and other antineoplastic agents.

2. Materials and Methods

Materials

Common reagents were purchased from Sigma-Aldrich (St. Louis, MO) and used as received unless otherwise specified. *N,N'*-dicyclohexylcarbodiimide (DCC), 4-(dimethylamino)pyridine (DMAP) were obtained from AAPPTEC (Louisville, KY). 2,2'-Azobis(2,4-dimethylvaleronitrile) (V-65) was from Wako USA (Richmond, VA). Paclitaxel (PTX, >99.5%) was purchased from LC Laboratories (Woburn, MA). ^{125}Iodine [^{125}I] was obtained from Perkin-Elmer (Waltham, MA). *N*-(2-hydroxypropyl)methacrylamide (HPMA) [29], *N*-methacryloylglycylphenylalanylleucylglycine (MA-GFLG-OH) [30], *N*-methacryloyltyrosinamide (MA-Tyr-NH_2) [31] and RAFT agents, 4-cyanopentanoic acid dithiobenzoate (CPA) [32] and peptide2CTA (N^{α},N^{ε}-bis(4-cyano-4-(phenylcarbonothioylthio)pentanoylglycylphenylalanylleucylglycyl)lysine) [24], were synthesized according to literature. 4,4'-Azobis(*N,N'*-propargyl-4-cyanopentanamide) (dialkyne-V-501) and N^{α},N^{δ}-(bis(azidobenzoylglycylphenylalanylleucylglycylalanyl)lysine (N_3-GFLG-N_3) were prepared according to described procedures [33].

Synthesis of Polymerizable Derivative of Paclitaxel (MA-GFLG-PTX)

Under nitrogen atmosphere, MA-GFLG-OH (5 g, 10.9 mmol), paclitaxel (9.3 g, 10.9 mmol), DMAP (1 g, 8.7 mmol) were dissolved in 25 mL of *N,N*-dimethylformamide (DMF). A tiny amount of *t*-octylpyrocatechine was added as inhibitor to avoid polymerization. The solution was cooled to 0 °C. DCC (3.4 g, 16.3 mmol) in DMF (5 mL) was added dropwise. The reaction mixture was kept under 4 °C for 24 h and then 2 h at room temperature. Dicyclohexylurea (DCU) was removed by filtration. The filtrate was evaporated in vacuum. The residue was redissolved in ethylacetate. Small amount of DCU was again removed by filtration. The filtrate was precipitated in ether. The crude product was purified by column chromatography (silica gel 60 Å, 200–400 mesh, ethyl acetate : acetone 8:1) to give white solid in 52.1% yield.

^{1}H NMR (DMSO-d_6, 400 MHz): d 69-0.78 (m, 6H, δ-Leu); 1.00 (m, 6H,16+17); 1.33 (m, 2H, β-Leu); 1.46 (s, 3H, 19); 1.61 (m, 1H, γ-Leu); 1.74 (m, 7H, 6+14+18); 2.06 (m, 6H, MA-C**H**$_3$ + C**H**$_3$COO-10); 2.20 (s, 3H, C**H**$_3$COO-4); 2.45-2.89 (m, 2H, β-Phe); 3.54 (m, 1H, 3); 3.69 (m, 2H, C**H$_2$**(Gly)); 3.89 (m, 2H, C**H$_2$**(Gly)); 3.98 (m, 2H, 20); 4.08 (m, 1H, 7); 4.15-4.25 (m, 1H, α-Leu); 4.50 (m, 1H, α-Phe); 4.57 (m, 1H, OH-1); 4.87 (m, 2H, 5+OH-7); 5.27 (s, 1H, CH=); 5.34 (m, 1H, 2'); 5.38 (d, 1H, 2); 5.46 (dd, 1H, 3'); 5.65 (s, 1H, CH=); 5.91 (t, 1H, 13); 6.26 (s, 1H, 10); 7.18 (m, 5H, Phe); 7.41 (m, 5H, arom-taxol); 7.64-7.52 (m, 5H, arom-taxol); 7.82-7.92 (m, 5H, arom taxol); 8.10 (m, 2H, N**H**-Phe + N**H**-Phe); 8.24 (m, 1H, N**H**-Gly-amide); 8.34 (m, 1H, N**H**-Glyester); 9.23 (d, 1H, N**H**-5' taxol).

Synthesis of Multiblock HPMA Copolymer-Paclitaxel Conjugate (mP-PTX)

Synthetic procedure consisted of two steps: RAFT copolymerization of HPMA with MA-GFLGPTX, followed by "click" reaction.

a. Synthesis of clickable telechelic HPMA copolymer-paclitaxel conjugate (tP-PTX)—HPMA (886 mg, 6.19 mmol), MA-GFLG-PTX (245 mg, 0.19 mmol) and MA-Tyr-NH_2 (15 mg, 0.06 mmol) were dissolved in methanol. The solution was bubbled with N_2 for 30 min. RAFT agent peptide2CTA and initiator V-65 were added via syringe. Polymerization took place at 50 °C for 40 h. The copolymer was precipitated in acetone, isolated by centrifugation and purified by dissolution-precipitation in methanol-acetone twice, then dried under vacuum at room temperature. The copolymer was obtained as a slightly pink powder; yield 454 mg (Mw 109 kDa, PDI 1.14). The product (440 mg) was further reacted with dialkyne-V-501 (61 mg, 0.17 mmol, over 20 times excess with respect

to the polymer end groups) in 4 mL DMF at 70 °C for 2 h, purified by precipitation into acetone twice, resulting in α,ω-dialkyne telechelic HPMA copolymer-paclitaxel conjugate.

b. Chain extension via Cu (I) assisted alkyne-azide click reaction and fractionation—Diazide-GFLGK (4.0 mg, 3.4 μmol), α,ω-dialkyne telechelic HPMA (350 mg, about 3.4 μmol), and sodium ascorbate (8 mg, 40 μmol) were put in a vial. The vial was evacuated and refilled with nitrogen three times before adding 1.1 mL of deoxygenated DMF. Deoxygenated solution of $CuSO_4$ (200 μL; 3.2 mg, 20 μmol) was added and the vial was sealed. The solution was stirred at room temperature for 20 h. The polymer was precipitated into acetone and dried under vacuum, and further fractionated/purified by size exclusion chromatography using a Superose 6 HR/16/30 column. After dialysis against water and freeze-drying, final product (Mw 335 kDa, PDI 1.09) was obtained (120 mg, 30% yield).

Similar procedure was followed to prepare biodegradable multiblock polyHPMA (mP) for *in vivo* control experiment.

Synthesis of Traditional HPMA Copolymer-Paclitaxel Conjugate (P-PTX)

To enable comparison of the activity of biodegradable multiblock HPMA copolymer-drug conjugate (mP-PTX) to that of a traditional HPMA copolymer-drug conjugate (P-PTX), a conjugate with Mw lower than 50 kDa was synthesized by RAFT copolymerization as described above but using CPA as the chain transfer agent. In a typical polymerization reaction, monomers (HPMA: 289 mg, 2 mmol; MA-GFLG-PTX: 82 mg, 0.063 mmol; MA-Tyr: 5 mg, 0.02 mmol) were dissolved in methanol under N_2 atomosphere. CPA and V-65 at a molar ratio of 4:1 were added through syringe. The ampoule was sealed and the polymerization was carried out at 50 °C for 40 h. The copolymer was precipitated in acetone, washed with acetone 3 times and dried under reduced pressure at room temperature. Yield 169 mg pink powder (45%) with Mw 48 kDa and PDI 1.05. The dithiobenzoate end group was removed by radical-induced modification with excess V-65 as previously reported [33].

Characterization of HPMA Copolymer-Paclitaxel Conjugates

The total content of PTX in P-PTX and mP-PTX was determined by enzyme-catalyzed cleavage of PTX from HPMA copolymer-PTX conjugates followed by HPLC analysis. Papain was used and the cleavage was performed in McIlvaine's buffer (50 mM citrate/0.1 M phosphate, pH 6.0) at 37 °C. An example is described as follows: To a conjugate solution in DMSO (50 mg/mL, 10 μL), glutathione (10 mM, 100 μL) and papain (25 mg/mL, 20 μL) in McIlvaine's buffer were added sequentially. The sample was incubated at 37 °C water bath for 4 h. Then 290 μL methanol containing 0.02% acetic acid was added. The sample was analyzed by HPLC (Agilent Technologies 1100 series, Zorbax C8 column 4.6×150 mm) using flow rate 1.0 mL/min and gradient elution from 30% to 90% of buffer B within 30 min (Buffer A: DI H_2O with 0.1% TFA, Buffer B: acetonitrile with 0.1% TFA). The amount of cleaved PTX was calculated based on a PTX standard calibration curve.

The molecular weight and polydispersity index (PDI) of polymers were measured on an ÄKTA FPLC system (GE Healthcare) equipped with miniDAWN TREOS and OptilabEX detectors (Wyatt Technology, Santa Barbara, CA) using a Superose 6 HR10/30 column with sodium acetate buffer containing 30% acetonitrile (pH 6.5) as mobile phase. HPMA homopolymer fractions were used as molecular weight standards.

The characteristics of conjugates are summarized in Table 1.

In Vitro Degradation of mP-PTX and Release of PTX from the Conjugates

The degradability of mP-PTX and the release of PTX from the polymer conjugates were investigated by incubation of the conjugates in McIlvaine's buffer (50 mM citrate/0.1 M phosphate; 2 mM EDTA, pH 6.0) at 37°C in the presence of papain (2.0 μM) with concentration of polymer 3 mg/mL for 12 h. At predetermined time points, a sample was withdrawn and analyzed by HPLC for drug release and by SEC for degradation. All degradation and cleavage determinations were carried out in duplicate.

Cell Culture and Transduction

A2780 and A2780/AD human ovarian cancer cells were obtained from American Type Cell Culture (Rockville, MD). Cells were maintained at 37 °C in a humidified atmosphere containing 5% CO_2 in RPMI-1640 medium (Gibco, Carlsbad, CA) supplemented with 10% fetal calf serum and a mixture of antibiotics (100 units/mL penicillin, 0.1 mg/mL streptomycin; Biochrom AG, Holliston, MA). A2780 drug-sensitive cells were incubated with F-Luc-IRES-mCherry lentivirus (Capital Biosciences, Rockville, MD) suspension in the presence of 8 mg/mL of polybrene (Millipore, Billerica, MA) for 24 h. The mCherry- & luciferase-positive cells were selected 48 h later by fluorescence-activated cell sorting (FACS) (>95%).

Cytotoxicity Study

The cytotoxicity of free PTX and its polymeric conjugates (P-PTX and mP-PTX) against A2780 drug-sensitive human ovarian cancer cells and A2780/AD drug-resistant human ovarian cancer cells was measured by Kit-8 assay (CCK-8, Dojindo, Japan). The cells were seeded in 96-well plates at the density of 10,000 cells/well in RMPI-1640 media containing 10% fetal bovine serum. After 24 h, media were replaced and media containing the conjugates were added. The cells were incubated with free PTX or its polymeric conjugates at a series of PTX concentrations. After 72 h of incubation, the number of viable cells was estimated using CCK-8 kit according to manufacturer's protocol. In brief, PTX/conjugate-containing medium was discarded and replaced with 100 μL fresh growth medium in each well, followed by the addition of 50 μL 5× diluted CCK-8 solution. Dehydrogenase activities in live cells converted the water-soluble tetrazolium salt WST-8 into a soluble yellow-color formazan dye. After the incubation of cells at 37°C, 5% CO_2 for 2 h, the absorbance was measured via a microplate reader at 450 nm (630 nm as reference). Untreated control cells were set as 100% viable.

Radiolabeling

The HPMA copolymer-PTX conjugates, containing tyrosine methyl ester in the side chains, were reacted with $Na^{125}I$ (Perkin Elmer, Waltham, MA) at room temperature in 0.01 M phosphate buffer containing chloramine-T for 30 min and then purified with Sephadex PD-10 columns (GE Healthcare Biosciences, Pittsburgh, PA). The specific activity of the hot samples was in the range 45−65 μCi/mg.

Tumor Models

All animal studies were carried out in accordance with the University of Utah IACUC guidelines under approved protocols. Transfected luciferase-expressing A2780 drug-sensitive ovarian cancer cells (0.5×10^6) in 10 μL of phosphate buffer saline were orthotopically inoculated beneath the left ovarian bursa of 6- to 8-week-old syngeneic female nude mice. To monitor the tumor growth, the mice were imaged twice weekly using a Xenogen IVIS 100 imaging system (Xenogen, Alameda, CA) according to manufacturer's instructions.

Pharmacokinetics and Biodistribution Study

For pharmacokinetic study, 6- to 8-week-old healthy female nude mice (22–25 g; Charles River Laboratories, Wilmington, MA) (n=5) were injected intravenously with ^{125}I-labeled HPMA copolymer-PTX conjugates P-PTX and mP-PTX, respectively (2 mg, 20 μCi/mouse). At predetermined intervals, blood samples (10 μL) were taken from the tail vein, and the radioactivity of each sample was measured with Minaxi Autogamma 5000 Series Gamma Counter (Packard, Downers Grove, IL). The blood pharmacokinetic parameters for the radiotracer were analyzed using a noncompartmental model with WinNonlin 5.0.1 software (Pharsight Corp., Palo Alto, CA). For biodistribution study, 6- to 8-week-old healthy female nude mice (22–25 g; Charles River Laboratories, Wilmington, MA) (n=5) were intravenously injected with ^{125}I-labeled HPMA copolymer-PTX conjugates P-PTX and mP-PTX, respectively (2 mg, 20 μCi/mouse). At 7 d and 21 d after administration, the mice were sacrificed. Various tissues (heart, liver, spleen, kidney, lung, stomach, intestine, muscle, bone, and brain) were removed, weighed, and counted for radioactivity with Minaxi Autogamma 5000 Series Gamma Counter. Uptake of the conjugates was calculated as the percentage of the injected dose per gram of tissue (% ID/g).

SPECT/CT Imaging

^{125}I-labeled HPMA copolymer-PTX conjugates P-PTX and mP-PTX (5 mg, 200 μCi/mouse) were injected intravenously via the tail vein into tumor-bearing mice, respectively. At 1 h, 24 h, 7 d and 21 d after administration, mice were anesthetized with 2% isoflurane gas (IMWI/VetOne, Meridian, ID) in oxygen and positioned prone on the scanner bed. SPECT/CT images of mice were acquired by using an Inveon trimodality PET/SPECT/CT scanner (Siemens Preclinical Solutions, Knoxville, TN). A sensor was used to monitor the respiration rate of mice under anesthesia (Biovet, France). CT images consisting of 220 degrees and 480 projections at each of 2 bed positions were acquired first. The exposure time was 135 msec with a detector setting at 80 kVp and 500 μA. Data was reconstructed onto a 416×416×752 image matrix using the COBRA software package (Exxim Computing Corporation, Pleasanton, CA). The effective image pixel size was 97 μm. SPECT data were acquired immediately following the CT using a single pinhole collimator with a detector radius of rotation at 35 mm. Images were acquired over 1.5 detector revolutions with 6° between each of 90 projections. A 90 mm bed travel was used. Each projection was acquired for 12 seconds, and the data were histogrammed with a window setting of 20–40 KeV. Reconstruction was performed using ordered subset expectation maximization 3D (OSEM3D) with 8 iterations and 6 subsets. Reconstructed images were analyzed and visualized using the Siemens Inveon Research Workplace (IRW) software.

In Vivo Antitumor Activity

The antitumor efficacy of P-PTX and mP-PTX was evaluated in female nude mice bearing orthotopic luciferase-expressing A2780 ovarian tumors according to two criteria: a) tumor growth delay and b) change in the abdominal circumference. Three weeks after inoculation, when the tumor reached approximately 4–5 mm in diameter, mice were randomly assigned to five groups. The mice in drug-treated group received a single intravenous injection of PTX vehicle (Cremophor EL®: ethanol 1:1 v/v), P-PTX or mP-PTX at a PTX equivalent dose of 20 mg/kg (n=6). The mice in the control groups received saline, or multiblock HPMA copolymer without drug (mP) at a dose corresponding to the amount of conjugates injected for the drugloaded formulations (n=5). The day that mice received treatment was set as day 0. To monitor the tumor growth, the mice were intravenously injected with D-luciferin (Biosynth, Switzerland) via tail vein at a dose of 100 mg/kg and subsequently imaged every 2 days from day 0 to day 26 using a Xenogen IVIS 100 imaging system. Images were obtained with a 13 cm field of view, binning (resolution factor) of 8 (medium), F stop = 1, exposure = 5 min. Data were analyzed using Living Image 3.2 Software

(Xenogen, Alameda, CA) and presented as the sum of all detected photons per second (units: photons/sec) for each mouse, from a constant sized Region of Interest (ROI) drawn over the mouse abdomen. In parallel, the abdominal circumference and body weight of mice were measured every day. The tumor volume, abdominal circumference and body weight at day 0 were normalized to 100%. All subsequent tumor volumes, abdominal circumference, and body weight were then expressed as the percentage relative to those at day 0. At the end of the experiment, the animals were sacrificed and the tumor mass was harvested, photographed and weighted. In addition, the major organs (liver, spleen and tumor) of mice were harvested, cryosectioned and stained with hematoxylin and eosin (H&E). The slices were examined under a microscope.

Statistical Analysis

Statistical analyses were done using a two-tailed unpaired Student's *t*-test, with p values of <0.05 indicating statistically significant differences.

3. Results and Discussion

Synthesis and Characterization of P-PTX and mP-PTX

Paclitaxel has been conjugated to hydrophilic polymers to improve its bioavailability. The most well-known examples are poly(L-glutamic acid)-paclitaxel conjugates [34] and HPMA copolymer-paclitaxel conjugates [35, 36] in which PTX was covalently bound to polymer precursors through an ester bond at its 2'-OH position via variable linkers. The significant synthetic feature in this study is the utilization of polymerizable PTX derivative and controlled polymerization chemistry (Figure 1). It provides a facile way to adjust PTX content in conjugate by changing the feed ratio. The resulting HPMA copolymer conjugates possess molecular weights close to the theoretical design and very narrow molecular weight distribution as shown in Table 1. Moreover, a new architecture of HPMA copolymer-PTX conjugates, biodegradable multiblock conjugates with long-circulation in bloodstream, has been designed and prepared.

When using a 2-arm RAFT chain transfer agent (peptide2CTA), HPMA monomer incorporated at both dithiobenzoate groups with identical efficiency during RAFT polymerization [24]. Incubation of the polymer with papain, a thiol proteinase with similar specificity as lysosomal proteinases, resulted in the decrease of the molecular weight to half of the original value. This suggests that the molecular weight of HPMA copolymer-drug conjugates is not limited to the currently used range of 40–65 kDa. Consequently, the initial (clickable) telechelic HPMA copolymer-PTX conjugate was designed with molecular weight of 100 kDa. Figure 2A shows SEC curves of the initial conjugate, a narrow fraction of the chain extended mP-PTX, and the final degradation product with Mw of 48 kDa. This demonstrated the ability of the mP-PTX to be degraded to the polymer fragments below the renal threshold, capable of glomerular filtration. Figure 2B reveals that the cumulative PTX release is similar for P-PTX and mP-PTX. The slight decrease in the rate of PTX release for mP-PTX is most probably due to the formation of a more compact coil due to hydrophobic interactions of PTX terminated side chains.

Cytotoxicity *in vitro*

To investigate the ability of HPMA copolymer-drug conjugates to inhibit tumor growth, we evaluated the *in vitro* cytotoxicity of free PTX, P-PTX and mP-PTX toward A2780 drug-sensitive and A2780/AD drug-resistant human ovarian cancer cells. As shown in Table 2, the conjugates were found to possess biological activity toward human ovarian carcinoma A2780 cells *in vitro*. Like free PTX, both P-PTX and mP-PTX exhibited a dose-dependent cytotoxicity against A2780 and A2780/AD cells: mP-PTX (IC_{50}= 0.30 ± 0.05 nM, 5.31 ±

0.98 μM) and P-PTX (IC_{50}= 0.24 ± 0.07 nM, 7.48 ± 3.17 μM) exhibited similar therapeutic effect as free PTX (IC_{50}= 0.21 ± 0.09 nM, 4.18 ± 2.61 μM), indicating that PTX attached to the HPMA copolymer was readily available to interact with cancer cells and retained its antimitotic potency. Moreover, all of three compounds were 10000-fold more effective in A2780 drug-sensitive cells than in A2780/AD drug-resistant cells. Part of this phenomenon is related to the fact that PTX is bound to the HPMA copolymer via an ester bond. Consequently, during the incubation with cancer cells part of the drug is released from the carrier by (pure, non-enzymatic) hydrolysis and the cells are in fact exposed to a mixture of free and polymer-bound drug. This is the case for all conjugates containing pH-sensitive bonds [37–39]; consequently, *in vivo* data are of crucial importance for the evaluation of the potency of such conjugates. As shown below, the mP-PTX conjugate possessed the highest anticancer activity, validating the design.

Pharmacokinetics, biodistribution and imaging studies of ^{125}I-labeled P-PTX and mP-PTX

The pharmacokinetic behavior of mP-PTX, P-PTX and Cremophor EL®-based PTX vehicle were compared. The blood (radio)activity-time profiles of P-PTX and mP-PTX conjugates in mice are illustrated in Figure 3A. A two-compartmental model was used to analyze the blood pharmacokinetics of P-PTX and mP-PTX. Mean pharmacokinetic parameters of mP-PTX and PPTX are summarized in Table 3 and those of the Cremophor EL®-based PTX vehicle are cited from a previous report by Sparreboom et al. [40]. The terminal biological half-life ($T_{1/2, \beta}$) of mP-PTX (27.5 h) was higher than that of P-PTX (13.3 h), PTX (2 h) and Cremphor EL (17 h). The total area under the blood concentration versus time curve (AUC) of mP-PTX (1074.27 %ID/mL) was significantly higher than that of P-PTX (420.95 %ID/mL) ($p<0.001$). In addition, the mean residence time (MRT) of mP-PTX was also significantly longer than that of P-PTX (39.26 h vs. 18.25 h) ($p<0.001$). The mean systemic clearance (CL) was significantly lower in mP-PTX as compared to P-PTX (0.09 mL/h vs. 0.24 mL/h) ($p<0.001$). The mean volume of distribution at steady state (Vss) of mP-PTX was significantly less than that of P-PTX (3.65 mL vs. 4.34 mL) ($p<0.01$). The mP-PTX with relatively high Mw was cleared more slowly from the blood than commercial PTX vehicle and P-PTX with low Mw, indicating that increased Mw can prolong blood circulation time *in vivo*. In general, it is believed that long-term exposure of cancer cells to the drug at modest concentrations would be more effective than a pulsed supply at a high concentration. In addition, antineoplastic agents, like PTX, are cell-growth-phase-specific or cell-cycle-specific, that is, they can exert effective actions on cells only during a specific phase of cell growth and proliferation. Hence, long retention time of drugs in circulation is considered to be crucial to cell-cycle-specific drugs for effective chemotherapy.

Figure 3B reveals biodistribution data of P-PTX and mP-PTX. At 7 d after intravenous injection, most conjugates were taken up by the liver and spleen, probably due to the hydrophobic nature of PTX – a finding that is consistent with previous reports [41]. The uptake of mP-PTX in the spleen and liver (29.87 %ID/g, 19.97 %ID/g) was significantly higher than that of P-PTX (9.36 %ID/g, 5.42 %ID/g), which might be attributed to larger size and higher PTX content of mP-PTX. Despite high accumulation in major organs, mP-PTX in the spleen and liver at day 21 (17.74 %ID/g, 8.91 %ID/g) was 2-fold less than at day 7 (29.87 %ID/g, 19.97 %ID/g), indicating its *in vivo* biodegradability. In all tissues except liver and spleen, the amounts of mP-PTX were low (<0.28 %ID/g). In addition, SPECT/CT imaging results (Figure 4) also showed that the signal intensity of mP-PTX significantly decreased from day 1 to day 21, further demonstrating that the biodegradable polymers can temporarily serve as drug carriers to deliver drugs to the tumor sites, and then be broken down spontaneously in a predetermined manner into by-products that are eliminated from the body.

SPECT/CT images (Figure 4) showed that ^{125}I-labeled mP-PTX had significantly higher activity in the blood pool, liver, and spleen over the entire study period than ^{125}I-labeled P-PTX, which is consistent with the pharmacokinetics and biodistribution data (Figure 3). As expected, high radioactivity signal in the bladder at 1 h after administration indicated that P-PTX was rapidly cleared from mice because its Mw is below renal threshold (~50 kDa). By day 1, the whole-body signal intensity in mice treated with P-PTX was much lower than that of the mice treated with mP-PTX. The short retention time of P-PTX in the circulation resulted in limited pharmaceutical efficiency. To address this issue, the polymeric drug carriers with relatively high Mw have to be developed, which makes it possible that a single administration will sustain for extended periods of time and lead to substantially enhanced drug accumulation in solid tumor [19, 20]. Long-circulating conjugates provide a concentration gradient between blood circulation and tumor for an extended period of time; consequently, extravasation via leaky tumor vasculature becomes more efficient. However, our recent study revealed that for polymer - hydrophobic drug conjugates the efficacy of conjugates increases with molecular weight, but only up to a certain limiting molecular weight [42]. In further studies we shall evaluate multiblock HPMA copolymer conjugates of Mw 100 – 200 kDa to determine the optimal Mw for PTX conjugates.

Low Mw P-PTX rapidly leaked into the tumor within 1 h following intravenous administration, while the accumulation of mP-PTX in the tumor was readily visualized 24 h after injection (Figure 4). In the future, attaching a targeting ligand to the conjugate mP-PTX may further augment drug localization in the tumor, as previously demonstrated with HPMA copolymer-PTX [36] and chlorin e_6 [43, 44] conjugates. Currently, the majority of patients with cancer will die due to the development of drug resistance. In general, drug resistance can arise due to abnormalities of pharmacokinetics, tumor microenvironment and cancer-cell-specificity. All of above influence the response to chemotherapy by principally affecting intracellular active drug concentrations, drug-target interactions, and target-mediated cell damage [45]. The increased circulation time and tumor accumulation through introduction of high Mw HPMA copolymer could increase exposure of tumor cells to the drug PTX (drug concentration × time of exposure), which might overcome drug resistance and result in enhanced therapeutic efficacy. An important factor for the enhanced efficacy of polymer-bound drugs is the fact that internalization via endocytosis can overcome the efflux pump-mediated drug resistance. Following endocytosis, the drug is released within lysosomes and diffuses into the cytoplasm in the perinuclear region of the cell at a distance from the efflux pumps [46, 47].

Antitumor activity *in vivo*

To evaluate antitumor activity, different formulations of PTX were intravenously injected at a single dose of 20 mg equivalent PTX/kg into mice bearing orthotopic A2780 human ovarian tumors which is known as a rapidly growing and highly invasive ovarian carcinoma model. Figure 5A shows the A2780 tumor growth curves after treatment with saline, multiblock HPMA copolymer carrier (mP), Cremphor EL-based PTX vesicle, P-PTX, and mP-PTX. The tumors in all drug-treated groups showed growth retardation when compared to the control tumors. Particularly, the tumors treated with mP-PTX exhibited a significantly stronger response than the tumors treated with saline only or mP ($p<0.05$). Notably, the tumors treated with mP-PTX grew slower than those treated with Cremphor EL-based PTX vesicle and P-PTX, although this could not be demonstrated statistically within the first 20 days. Significant difference occurred after day 20 ($p<0.01$). A reason for this may be the lag time required for ovarian micro-environment and injected cancer cells to exhibit influences and interactions based on different mechanisms by which the local biochemical and mechanical microenvironment, which is comprised of various signaling molecules, cell types and the extracellular matrix (ECM), affects the progression of cancerous cells. At the

end of this *in vivo* experiment, the tumors of all different groups were removed and photographed. The tumor sizes were proportional to the signal intensities observed from bioluminescence imaging (Figure 5A, 5B). The tumors in mice treated with mP-PTX were obviously smaller when compared with the tumors from other treatment groups and controls. In this study, mP-PTX induced a significant delay in tumor growth, but was unable to provide complete tumor regression, probably due to the single low dose treatment applied within this experimental setting. Still, these results provide evidence for the therapeutic superiority of this high Mw formulation, which has demonstrated a better therapeutic index than PTX and P-PTX.

In addition, we also monitored abdominal circumference curves which to some extent reflect disease progression including features such as ascites accumulation and increased, intraperitoneal tumor burden (Figure 5C) [48]. Abdominal circumference increased more rapidly in control mice treated with saline or mP, when compared with mice in the drug-treated groups. The mice treated with mP-PTX displayed less fluctuation in abdominal circumference than those in other groups. After 26 d of treatment, all mice were sacrificed and dissected. Similar to human patients suffering from advanced diseases, metastatic tumors were found on the peritoneal surface, intestinal surface, and invading the uterus in all drug-treated and control groups. However, in the control groups, tumors were also found on the diaphragm and in the hilus of the liver. Moreover, all the mice treated with saline or mP developed bloody ascites, whereas all 5 mice treated with mP-PTX had no detectable ascites. The antitumor effect of mPPTX was also confirmed by the histological appearance of tumor tissue from the mice treated with mP-PTX (Figure 6). The tumor cells treated with mP-PTX displayed pyknosis of nuclei and condensation of the cytoplasm, which are typical features of apoptotic cell death. In contrast, significantly less apoptotic cells were observed in saline-treated tumors.

Toxicity

It is well known that the current PTX formulation containing Cremophor EL vesicle exerts a range of biological effects, such as severe anaphylactoid hypersensitivity reactions, hyperlipidemia, erythrocyte aggregation, and peripheral neuropathy [49]. Furthermore, Cremophor EL-based micelles may interact favorably with systemic mediators that are involved in the classical complement activation pathway [50]. Here, a single injection of different PTX formulations was given and then followed by daily monitoring of body weight. The body weight curve in Figure 5D demonstrated that free PTX induced significant body weight loss during the first week following administration, which was not attributed to disease progression but to drug exposure, whereas P-PTX only caused a negligible weight loss and mP-PTX did not cause any weight loss effects at all, indicating the excellent tolerability of this drug regimen. During the entire study period, the treatment with mP-PTX did not lead to any significant differences in body weight change when compared with saline and mP control groups. By day 26, the mPPTX treated mice gained an average of 13.3% body weight, while the mice treated with saline and mP gained 15.2% and 16.3%, respectively. The slight difference of body weights between control and mP-PTX treated groups may be attributed to the difference of tumor weight and ascites. In addition, chronic toxicity of mP-PTX was evaluated using histological analysis on day 26 after injection. In parallel, H&E stained sections of major organs (spleen and liver) with high accumulation of mP-PTX were examined. Figure 6 shows that the histopathologic features in the liver and spleen of mice treated with mP-PTX were similar to those observed in the saline-treated mice and no abnormal features were identified, indicating that mP-PTX showed no toxicity when administered at a single dose of 20 mg equivalent PTX/kg. According to these findings, the biodegradable conjugate proved to be safe after single bolus injection, allowing the delivery of PTX doses exceeding those of the commercial PTX formulations. In the

future studies, we would like to propose the detailed evaluation of repetitive, increased doses of mP-PTX in tumor-bearing mice and carriers of varying molecular weight as well as their combination with targeting ligands.

4. Conclusions

We designed and synthesized a backbone biodegradable multiblock HPMA copolymer-PTX conjugate mP-PTX. The study demonstrated that the delivery of PTX mediated by multiblock backbone biodegradable high Mw (335 kDa) polymer carrier did result in prolonged blood circulation time and enhanced antitumor efficacy as compared to Cremphor EL-based PTX vesicle and low Mw (48 kDa) HPMA copolymer-PTX conjugate P-PTX. The data also indicate that backbone biodegradable mP-PTX conjugate exhibited less systemic toxicity than free PTX and P-PTX. Moreover, it was demonstrated that mP-PTX was degraded and cleared from the body. Thus, we anticipate that this new drug delivery system can open up new opportunities to improve current cancer chemotherapy.

Acknowledgments

The authors thank Brian Watson and Professor Edward W. Hsu for assisting the SPECT/CT imaging study and Tian Yu for the assistance with PK analysis. This work was supported in part by NIH grant CA156933 (to JK) from the National Cancer Institute.

References

1. Feng SS. Nanoparticles of biodegradable polymers for new-concept chemotherapy. Expert Rev. Med. Devices. 2004; 1:115–125. [PubMed: 16293015]
2. Ho EA, Vassileva V, Allen C, Piquette-Miller M. In vitro and in vivo characterization of a novel biocompatible polymer-lipid implant system for the sustained delivery of paclitaxel. J. Control. Release. 2005; 104:181–191. [PubMed: 15866344]
3. Sandercock J, Parmar MK, Torri V, Qian W. First-line treatment for advanced ovarian cancer: paclitaxel, platinum and the evidence. Br. J. Cancer. 2002; 87:815–824. [PubMed: 12373593]
4. Friedrich M, Diesing D, Villena-Heinsen C, Felberbaum R, Kolberg HC, Diedrich K. Taxanes in the first-line chemotherapy of metastatic breast cancer: review. Eur. J. Gynaecol. Oncol. 2004; 25:66–70. [PubMed: 15053065]
5. Keresztes RS, Port JL, Pasmantier MW, Korst RJ, Altorki NK. Preoperative chemotherapy for esophageal cancer with paclitaxel and carboplatin: results of a phase II trial. J. Thorac. Cardiovasc. Surg. 2003; 126:1603–1608. [PubMed: 14666040]
6. Bajetta E, Del Vecchio M, Bernard-Marty C, Vitali M, Buzzoni R, Rixe O, Nova P, Aglione S, Taillibert S, Khayat D. Metastatic melanoma: chemotherapy. Semin. Oncol. 2002; 29:427–445. [PubMed: 12407508]
7. Spencer CM, Faulds D. Paclitaxel. A review of its pharmacodynamic and pharmacokinetic properties and therapeutic potential in the treatment of cancer. Drugs. 1994; 48:794–847. [PubMed: 7530632]
8. Sparreboom A, van Tellingen O, Nooijen WJ, Beijnen JH. Tissue distribution, metabolism and excretion of paclitaxel in mice. Anticancer Drugs. 1996; 7:78–86. [PubMed: 8742102]
9. Weiss RB, Donehower RC, Wiernik PH, Ohnuma T, Gralla RJ, Trump DL, Baker JR Jr. Van Echo DA, Von Hoff DD, Leyland-Jones B. Hypersensitivity reactions from taxol. J. Clin. Oncol. 1990; 8:1263–1268. [PubMed: 1972736]
10. Xie Z, Guan H, Chen X, Lu C, Chen L, Hu X, Shi Q, Jing X. A novel polymer-paclitaxel conjugate based on amphiphilic triblock copolymer. J. Control. Release. 2007; 117:210–216. [PubMed: 17188776]
11. Biswas S, Dodwadkar NS, Deshpande PP, Torchilin VP. Liposomes loaded with paclitaxel and modified with novel triphenylphosphonium-PEG-PE conjugate possess low toxicity, target

mitochondria and demonstrate enhanced antitumor effects in vitro and in vivo. J. Control. Release. 2012; 159:393–402. [PubMed: 22286008]

12. Joshi N, Shanmugam T, Kaviratna A, Banerjee R. Proapoptotic lipid nanovesicles: synergism with paclitaxel in human lung adenocarcinoma A549 cells. J. Control. Release. 2011; 156:413–420. [PubMed: 21807043]
13. Zhang P, Hu L, Yin Q, Zhang Z, Feng L, Li Y. Transferrin-conjugated polyphosphoester hybrid micelle loading paclitaxel for brain-targeting delivery: synthesis, preparation and in vivo evaluation. J. Control. Release. 2012; 159:429–434. [PubMed: 22306333]
14. Cirstoiu-Hapca A, Buchegger F, Lange N, Bossy L, Gurny R, Delie F. Benefit of anti-HER2-coated paclitaxel-loaded immuno-nanoparticles in the treatment of disseminated ovarian cancer: Therapeutic efficacy and biodistribution in mice. J. Control. Release. 2010; 144:324–331. [PubMed: 20219607]
15. Roger E, Lagarce F, Garcion E, Benoit JP. Lipid nanocarriers improve paclitaxel transport throughout human intestinal epithelial cells by using vesicle-mediated transcytosis. J. Control. Release. 2009; 140:174–181. [PubMed: 19699246]
16. Danhier F, Lecouturier N, Vroman B, Jerome C, Marchand-Brynaert J, Feron O, Preat V. Paclitaxel-loaded PEGylated PLGA-based nanoparticles: in vitro and in vivo evaluation. J. Control. Release. 2009; 133:11–17. [PubMed: 18950666]
17. Sugahara S, Kajiki M, Kuriyama H, Kobayashi TR. Complete regression of xenografted human carcinomas by a paclitaxel-carboxymethyl dextran conjugate (AZ10992). J. Control. Release. 2007; 117:40–50. [PubMed: 17126446]
18. Seymour LW, Duncan R, Strohalm J, Kopeček J. Effect of molecular weight of *N*-(2-hydroxypropyl)methacrylamide copolymers on body distribution and rate of excretion after subcutaneous, intraperitoneal and intravenous administration. J Biomed. Mater. Res. 1987; 21:1341–1358. [PubMed: 3680316]
19. Maeda H. Tumor-selective delivery of macromolecular drugs via the EPR effect: background and future prospects. Bioconjug. Chem. 2010; 21:797–802. [PubMed: 20397686]
20. Allmeroth M, Moderegger D, Biesalski B, Koynov K, Rösch F, Thews O, Zentel R. Modifying the body distribution of HPMA-based copolymers by molecular weight and aggregate formation. Biomacromolecules. 2011; 12:2841–2849. [PubMed: 21692523]
21. Etrych T, Šubr V, Strohalm J, Šírová M, Říhová B, Ulbrich K. HPMA copolymer-doxorubicin conjugates: The effects of molecular weight and architecture on biodistribution and in vivo study. J. Control. Release. 2012
22. Yang J, Luo K, Pan H, Kopečková P, Kopeček J. Synthesis of biodegradable multiblock copolymers by click coupling of RAFT-generated heterotelechelic polyHPMA conjugates. React. Funct. Polym. 2011; 71:294–302. [PubMed: 21499527]
23. Luo K, Yang J, Kopečková P, Kopeček J. Biodegradable multiblock poly[*N*-(2-hydroxypropyl)methacrylamide] via reversible addition-fragmentation chain transfer polymerization and click chemistry. Macromolecules. 2011; 44:2481–2488. [PubMed: 21552355]
24. Pan H, Yang J, Kopečková P, Kopeček J. Backbone degradable multiblock *N*-(2-hydroxypropyl)methacrylamide copolymer conjugates via reversible addition-fragmentation chain transfer polymerization and thiol-ene coupling reaction. Biomacromolecules. 2011; 12:247–252. [PubMed: 21158387]
25. Wang Z, Hu X, Yue J, Jing X. Experimental study on biodegradable polymer-paclitaxel conjugate micelles for chemotherapy of C6 glioma. J. Control. Release. 2011; 152(Suppl 1):e41–e42. [PubMed: 22195914]
26. Yang R, Meng F, Ma S, Huang F, Liu H, Zhong Z. Galactose-decorated cross-linked biodegradable poly(ethylene glycol)-*b*-poly(ε-caprolactone) block copolymer micelles for enhanced hepatoma-targeting delivery of paclitaxel. Biomacromolecules. 2011; 12:3047–3055. [PubMed: 21726090]
27. You J, Shao R, Wei X, Gupta S, Li C. Near-infrared light triggers release of Paclitaxel from biodegradable microspheres: photothermal effect and enhanced antitumor activity. Small. 2010; 6:1022–1031. [PubMed: 20394071]

28. Yu DH, Lu Q, Xie J, Fang C, Chen HZ. Peptide-conjugated biodegradable nanoparticles as a carrier to target paclitaxel to tumor neovasculature. Biomaterials. 2010; 31:2278–2292. [PubMed: 20053444]
29. Kopeček J, Bažilová H. Poly[*N*-(2-hydroxypropyl)methacrylamide]. 1. Radical polymerization and copolymerization. Europ. Polym. J. 1973; 9:7–14.
30. Rejmanová P, Pohl J, Baudyš M, Kostka V, Kopeček J. Polymers containing enzymatically degradable bonds. 8. Degradation of oligopeptide sequences in *N*-(2-hydroxypropyl)methacrylamide copolymers by bovine spleen cathepsin B. Makromol. Chem. 1983; 184:2009–2020.
31. Duncan R, Cable HC, Rejmanová P, Kopeček J, Lloyd JB. Tyrosinamide residues enhance pinocytic capture of*N*-(2-hydroxypropyl)methacrylamide copolymers. Biochim. Biophys. Acta. 1984; 799:1–8. [PubMed: 6722178]
32. Mitsukami Y, Donovan MS, Lowe AB, McCormick CL. Water-soluble polymers. 81. Direct synthesis of hydrophilic styrenic-based homopolymers and block copolymers in aqueous solution via RAFT. Macromolecules. 2001; 34:2248–2256.
33. Pan, H.; Yang, J.; Kopečková, P.; Luo, K.; Kopeček, J. Polymeric drug delivery conjugates and methods of making and using thereof. US Patent Appl. 24U03.1-500 (Filed 03/08/2010).
34. Chipman SD, Oldham FB, Pezzoni G, Singer JW. Biological and clinical characterization of paclitaxel poliglumex (PPX, CT-2103), a macromolecular polymer-drug conjugate. Int. J. Nanomedicine. 2006; 1:375–383. [PubMed: 17722272]
35. Erez R, Segal E, Miller K, Satchi-Fainaro R, Shabat D. Enhanced cytotoxicity of a polymer-drug conjugate with triple payload of paclitaxel. Bioorg. Med. Chem. 2009; 17:4327–4335. [PubMed: 19482477]
36. Journo-Gershfeld G, Kapp D, Shamay Y, Kopeček J, David A. Hyaluronan oligomers-HPMA copolymer conjugates for targeting paclitaxel to CD44-overexpressing ovarian carcinoma. Pharmaceutical Res. 2012; 29:1121–1133.
37. Choi W-M, Kopečková P, Minko T, Kopeček J. Synthesis of HPMA copolymer containing Adriamycin bound via an acid-labile spacer and its activity toward human ovarian carcinoma cells. J. Bioact. Compat. Polym. 1999; 14:447–456.
38. Etrych T, Šírová M, Starovoytova L, Říhová B, Ulbrich K. HPMA copolymer conjugates of paclitaxel and docetaxel with pH-controlled drug release. Mol. Pharmaceutics. 2010; 7:1015–1026.
39. Šírová M, Mrkvan T, Etrych T, Chytil P, Rossmann P, Ibrahimova M, Kovář L, Ulbrich K, Říhová B. Preclinical evaluation of linear HPMA-doxorubicin conjugates with pH-sensitive drug release: efficacy, safety, and immunomodulating activity in murine model. Pharmaceutical Res. 2010; 27:200–208.
40. Sparreboom A, van Tellingen O, Nooijen WJ, Beijnen JH. Nonlinear pharmacokinetics of paclitaxel in mice results from the pharmaceutical vehicle Cremophor EL. Cancer Res. 1996; 56:2112–2115. [PubMed: 8616858]
41. Li C, Newman RA, Wu QP, Ke S, Chen W, Hutto T, Kan Z, Brannan MD, Charnsangavej C, Wallace S. Biodistribution of paclitaxel and poly(L-glutamic acid)- paclitaxel conjugate in mice with ovarian OCa-1 tumor. Cancer Chemother. Pharmacol. 2000; 46:416–422. [PubMed: 11127947]
42. Pan H, Sima M, Yang J, Kopeček J. Synthesis of long-circulating backbone degradable HPMA copolymer-doxorubicin conjugates and evaluation of molecular weight dependent antitumor efficacy. submitted.
43. Shiah J-G, Sun Y, Kopečková P, Peterson CM, Straight RC, Kopeček J. Combination chemotherapy and photodynamic therapy of targetable*N*-(2-hydroxypropyl)methacrylamide copolymer – doxorubicin/mesochlorin e_6 - OV-TL16 antibody immunoconjugates. J. Control. Release. 2001; 74:249–253. [PubMed: 11489502]
44. Lu Z-R, Shiah J-G, Kopečková P, Kopeček J. Polymerizable Fab' antibody fragment targeted photodynamic cancer therapy in nude mice. STP Pharma Sci. 2003; 13:69–75.
45. Agarwal R, Kaye SB. Ovarian cancer: strategies for overcoming resistance to chemotherapy. Nat. Rev. Cancer. 2003; 3:502–516. [PubMed: 12835670]

46. Minko T, Kopečková P, Kopeček J. Efficacy of chemotherapeutic action of HPMA copolymer-bound doxorubicin in a solid tumor model of ovarian carcinoma. Int. J. Cancer. 2000; 86:108–117. [PubMed: 10728603]

47. Minko T. HPMA copolymers for modulating cellular signaling and overcoming multidrug resistance. Adv. Drug Delivery Rev. 2010; 62:192–202.

48. Hu L, Zaloudek C, Mills GB, Gray J, Jaffe RB. In vivo and in vitro ovarian carcinoma growth inhibition by a phosphatidylinositol 3-kinase inhibitor (LY294002). Clin. Cancer Res. 2000; 6:880–886. [PubMed: 10741711]

49. Gelderblom H, Verweij J, Nooter K, Sparreboom A. Cremophor EL: the drawbacks and advantages of vehicle selection for drug formulation. Eur. J. Cancer. 2001; 37:1590–1598. [PubMed: 11527683]

50. Le Garrec D, Gori S, Luo L, Lessard D, Smith DC, Yessine MA, Ranger M, Leroux JC. Poly(*N*-vinylpyrrolidone)-*block*-poly(D,L-lactide) as a new polymeric solubilizer for hydrophobic anticancer drugs: in vitro and in vivo evaluation. J. Control. Release. 2004; 99:83–101. [PubMed: 15342183]

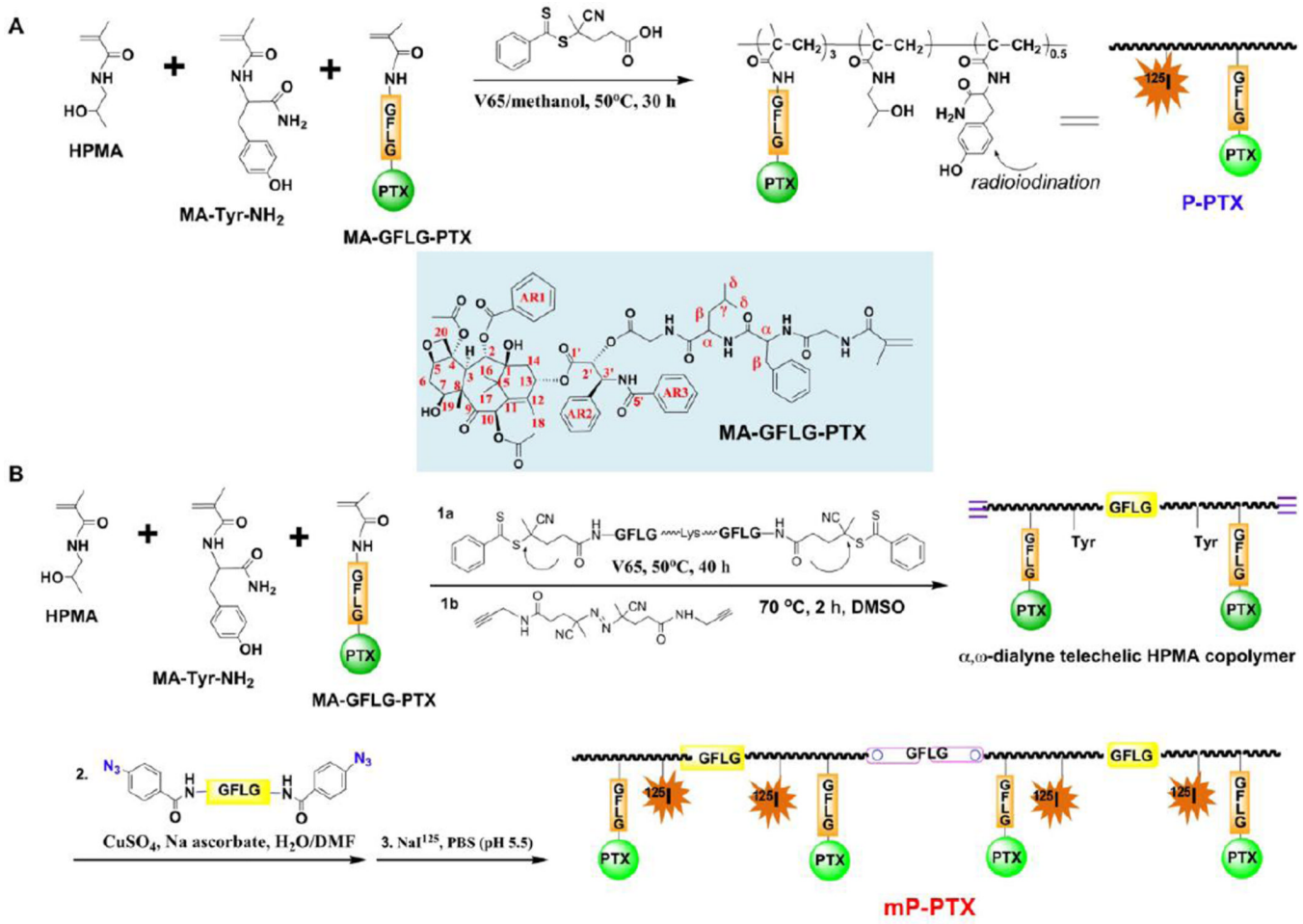

Figure 1.

Synthetic scheme of multiblock backbone biodegradable HPMA copolymer-PTX conjugates. (A) Synthesis of traditional HPMA copolymer-paclitaxel conjugate (PPTX). (B) Synthesis of multiblock HPMA copolymer-paclitaxel conjugate (mP-PTX).

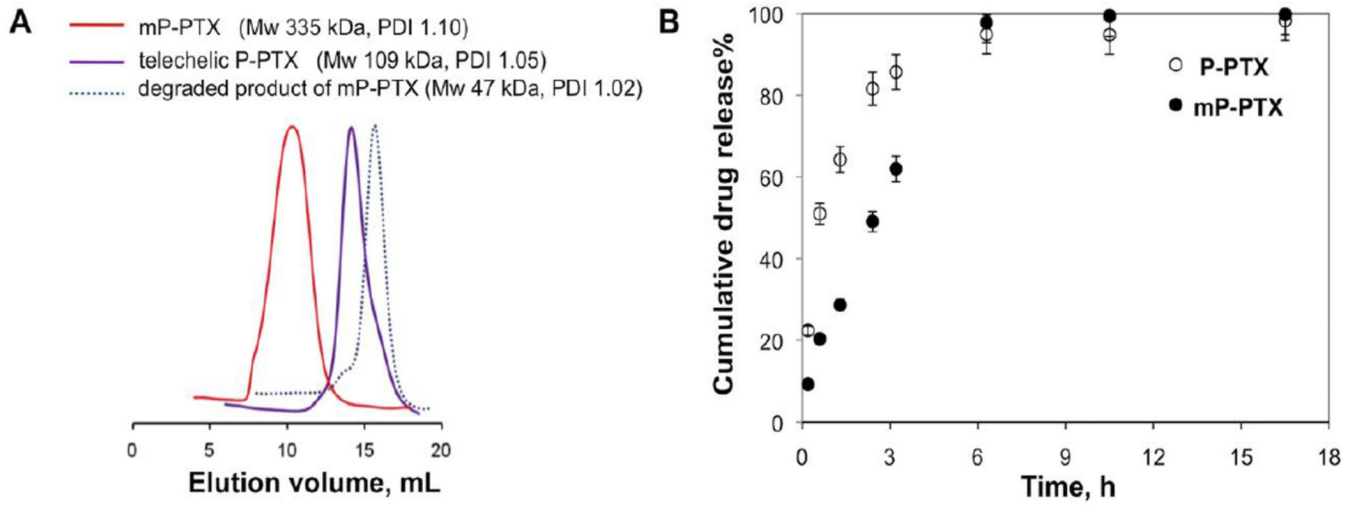

Figure 2.

(A) SEC profiles of telechelic tP-PTX (Mw 109 kDa); multiblock backbone biodegradable HPMA copolymer-PTX conjugate mP-PTX (fraction Mw 335 kDa); and of the degradation product (Mw 48 kDa) after incubation of mP-PTX solution (3 mg/mL) with 1 μM papain for 3 h at 37 °C. (B) Cumulative PTX release from P-PTX and mP-PTX (3 mg/mL) by 2 μM papain at 37 °C.

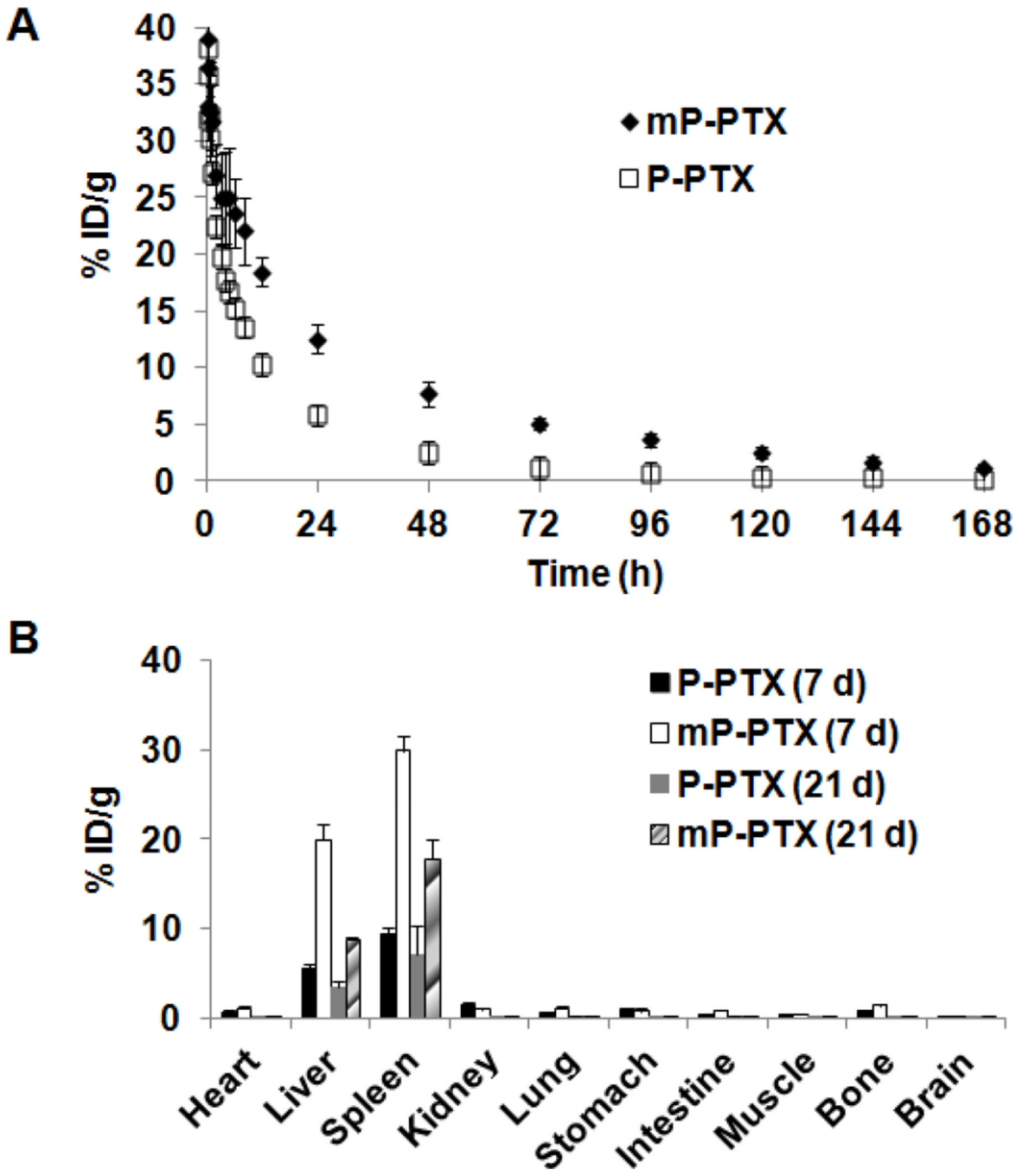

Figure 3.

(A) Blood activity-time profiles of ^{125}I-labeled P-PTX or mP-PTX. The open circles represent the mean radioactivity expressed as a percentage of the injected dose per gram of blood from mice (n=5). (B) Biodistribution in female nude mice at 7 d and 21 d after intravenous injection of ^{125}I-labeled P-PTX or mP-PTX. Data obtained using the radioactivity count method plotted as percentage of injected dose per gram of tissue (%ID/g). All the data are expressed as mean ± standard deviation (n=4–5).

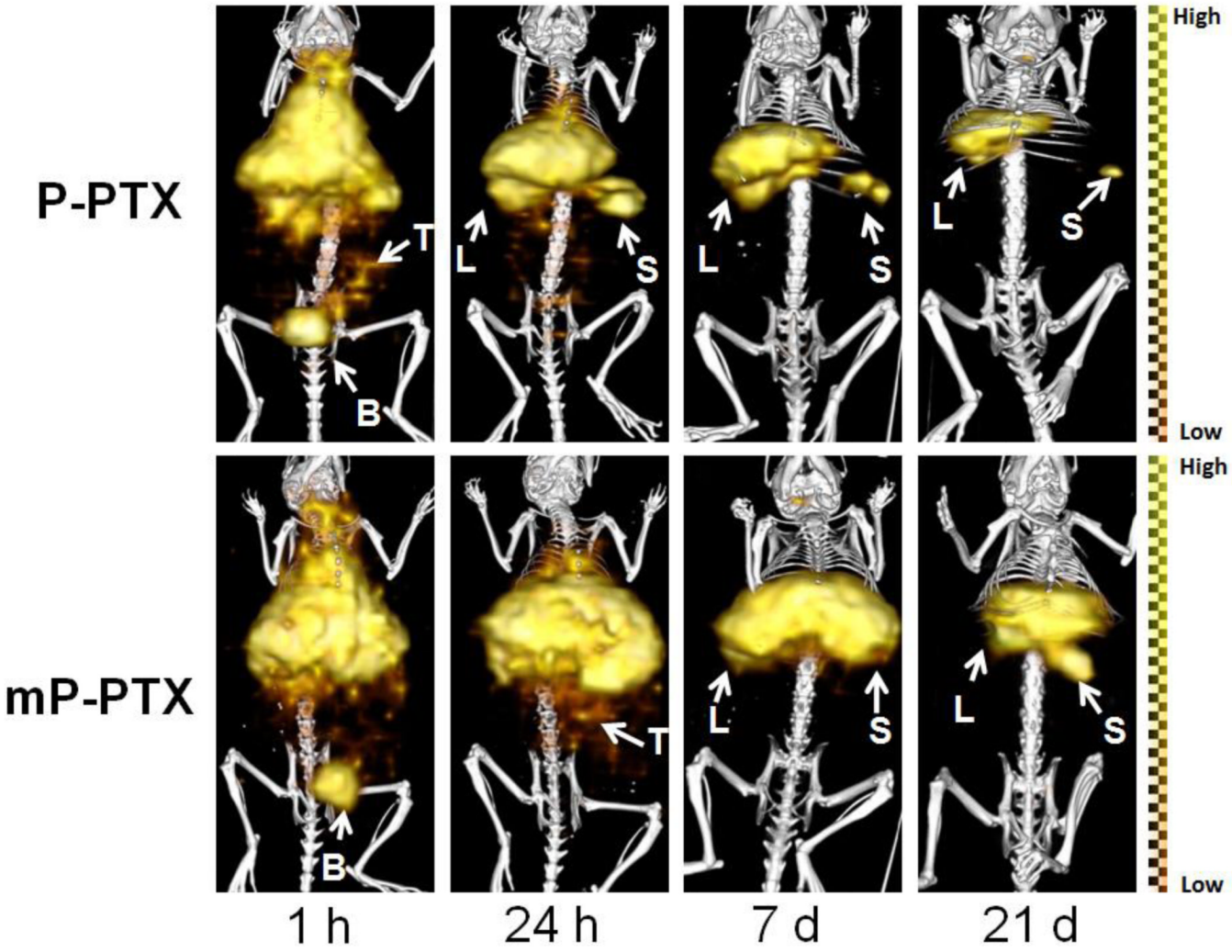

Figure 4.
SPECT/CT imaging of mice bearing orthotopic A2780 human ovarian carcinoma after intravenous injection of ^{125}I-labeled P-PTX or mP-PTX. The representative images were acquired 1 h, 24 h, 7 d, and 21 d after administration of conjugates. L, liver; S, spleen; B, bladder; T, tumor.

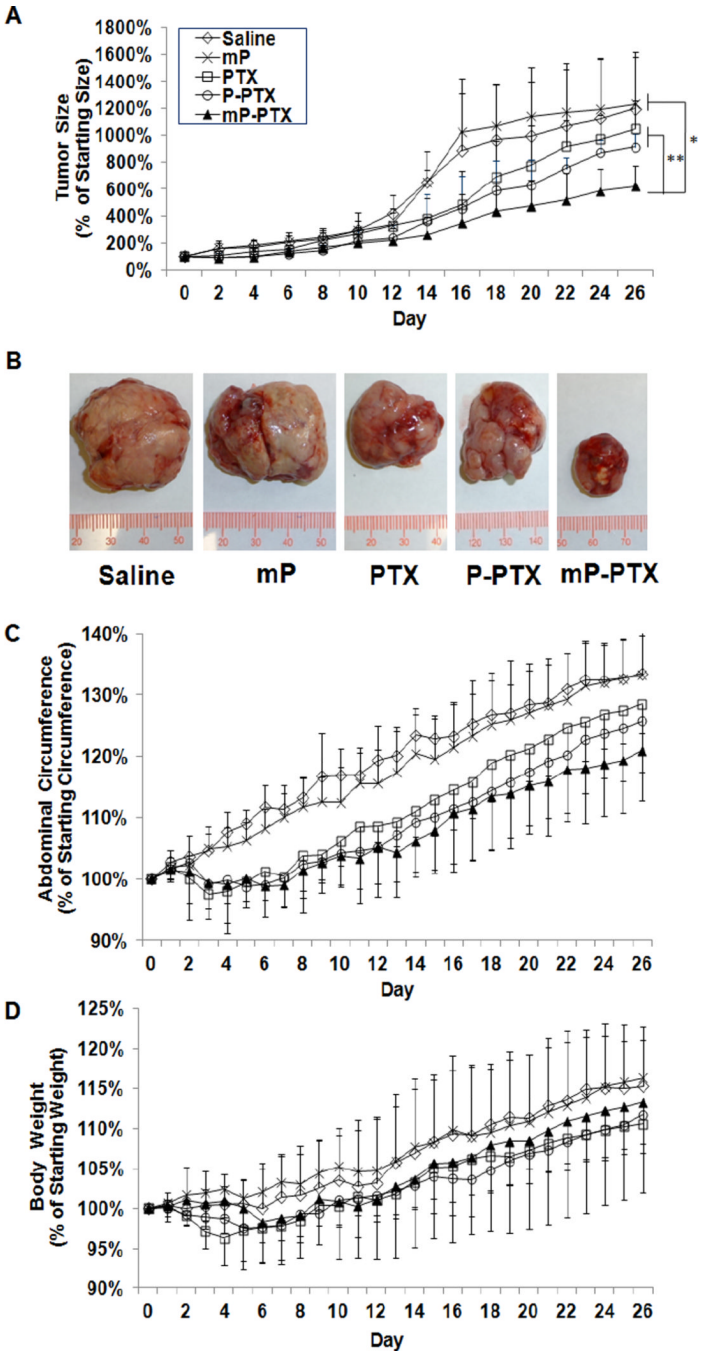

Figure 5.

In vivo antitumor activity against orthotopic A2780 human ovarian tumor. (A) A2780 tumor growth in mice treated with single dose of saline, mP, PTX, P-PTX, and mP-PTX at the dose of 20 mg equivalent PTX/kg. (B) Photographs of A2780 tumors after treatment with different PTX formulations. (C) Percentage of mean abdominal circumference change. (D) Percentage of mean body weight change. The data are presented as mean ± standard deviation (n=4–6).

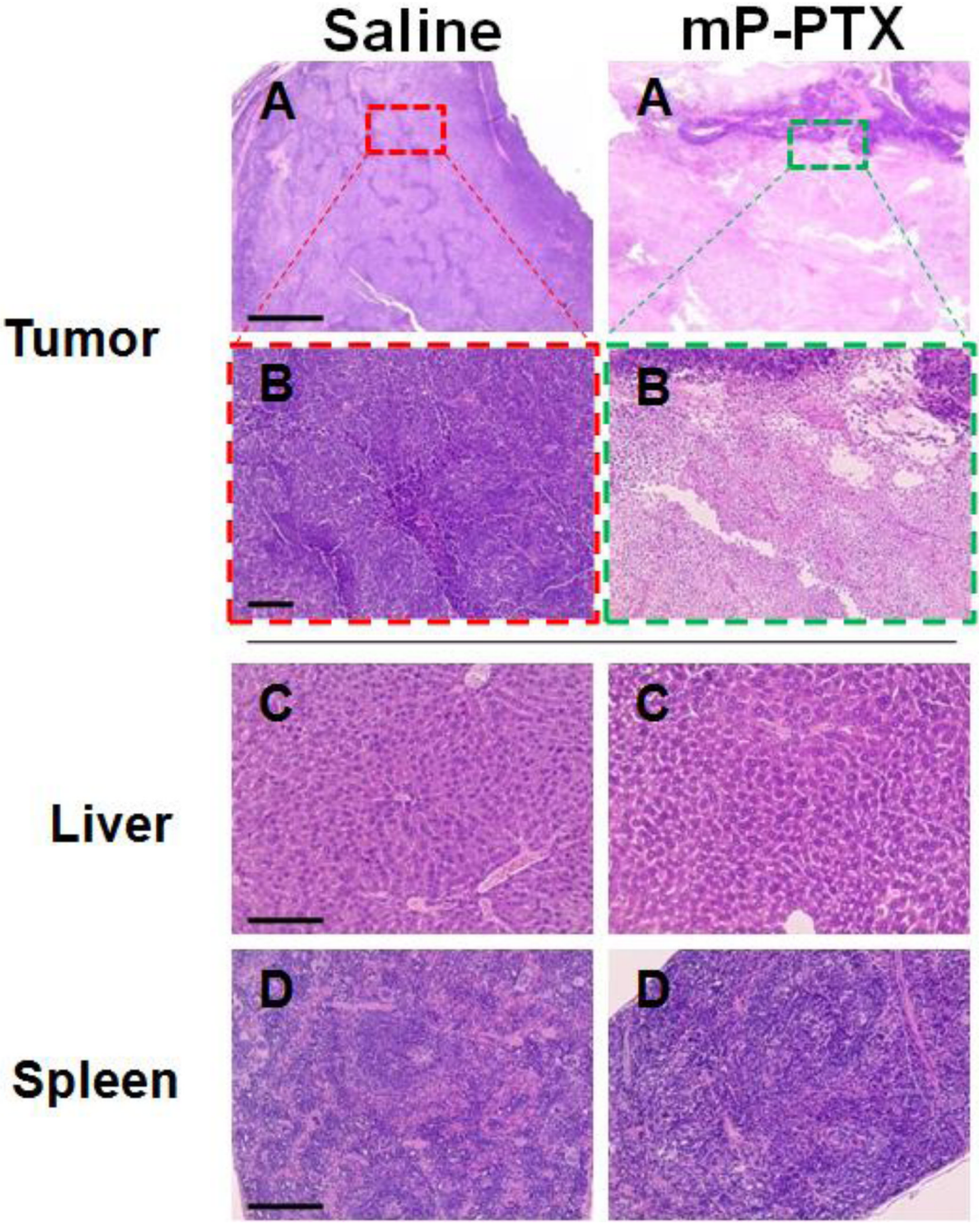

Figure 6.
Histological evaluation of tissue from A2780 tumor-bearing mice treated with saline (control) and mP-PTX (single dose at 20 mg equivalent PTX/kg). The tissues were sliced with 5-μm thickness and stained with hematoxylin and eosin (H&E). (A, B) Microphotographs of tumor after treatment for antitumor evaluation. (C, D) Microphotographs of liver and spleen for safety evaluation.

Table 1

Physicochemical properties of conjugates P-PTX and MP-PTX.

Polymer/ conjugate	CTA	Mn_{theory}, KDa	Found by SEC (kDa)			PTX (wt%)	Degradabilty
			Mn	Mw	Mw/Mn		
P-PTX	4-cyanopentanoic acid dithiobenzoate	50	46	48	1.05	7.3	no
tP-PTX	peptide2CTA	120	103	109	1.14	ND	yes
mP-PTX	peptide2CTA	clicked/ fractionated	306	335	1.09	4.2	yes
polyHPMA	peptide2CTA	clicked/ fractionated	291	324	1.11	N/A	yes

Table 2

IC_{50} values for free PTX, P-PTX and mP-PTX.

	A2780(nM)	A2780/AD (μM)
PTX	0.21 ± 0.09	4.18 ± 2.61
P-PTX	0.24 ± 0.07	7.48 ± 3.17
mP-PTX	0.30 ± 0.05	5.31 ± 0.98

Table 3

Comparison of pharmacokinetic parameters for ^{125}I-labeled P-PTX and mP-PTX in mice. $T_{1/2,\alpha}$ = initial half-life; $T_{1/2,\beta}$ = terminal half-life; AUC = total area under the blood concentration versus time curve; %ID = percentage of injected dose; CL = total body clearance; MRT = mean residence time; Vss = steady-state volume of distribution. Data are presented as mean ± standard deviation (n=5).

	P-PTX	mP-PTX
$T_{1/2,\alpha}$ (h)	0.88 ± 0.11	0.72 ± 0.19
$T_{1/2,\beta}$ (h)	13.30 ± 1.28	27.52±2.31***
AUC (%ID h/ml blood)	420.95±26.05	1074.27±72.03***
CL(mL/h)	0.24 ± 0.01	0.09 ± 0.01***
MRT(h)	18.25 ± 1.71	39.26±3.27***
Vss(mL)	4.34 ± 0.16	3.65 ± 0.09***

** indicates $p < 0.01$ and

*** indicates $p < 0.001$.